

# Decoupling Physical from Biological Processes to Assess the Impact of Viruses on a Mesoscale Algal Bloom

Yoav Lehahn,<sup>1</sup> Ilan Koren,<sup>1,\*</sup> Daniella Schatz,<sup>2</sup> Miguel Frada,<sup>2</sup> Uri Sheyn,<sup>2</sup> Emmanuel Boss,<sup>3</sup> Shai Efrati,<sup>4</sup> Yinon Rudich,<sup>1</sup> Miri Trainic,<sup>1</sup> Shlomit Sharoni,<sup>1,2</sup> Christian Laber,<sup>5</sup> Giacomo R. DiTullio,<sup>6</sup> Marco J.L. Coolen,<sup>7</sup> Ana Maria Martins,<sup>8</sup> Benjamin A.S. Van Mooy,<sup>7</sup> Kay D. Bidle,<sup>5</sup> and Assaf Vardi<sup>2,\*</sup>

<sup>1</sup>Department of Earth and Planetary Sciences, Weizmann Institute of Science, Rehovot 76100, Israel

<sup>2</sup>Department of Plant Sciences, Weizmann Institute of Science, Rehovot 76100, Israel

<sup>3</sup>School of Marine Science, University of Maine, Orono, ME 04469-5706, USA

<sup>4</sup>Department of Geophysical, Atmospheric and Planetary Sciences, Tel Aviv University, Tel Aviv 6997801, Israel

<sup>5</sup>Institute of Marine and Coastal Sciences, Rutgers University, New Brunswick, NJ 08901, USA

<sup>6</sup>Hollings Marine Laboratory, College of Charleston, Charleston, SC 29412, USA

<sup>7</sup>Marine Chemistry and Geochemistry Department, Woods Hole Oceanographic Institution, Woods Hole, MA 02543, USA

<sup>8</sup>University of the Azores, Horta, Azores 9901-862, Faial, Portugal

## Summary

Phytoplankton blooms are ephemeral events of exceptionally high primary productivity that regulate the flux of carbon across marine food webs [1–3]. Quantification of bloom turnover [4] is limited by a fundamental difficulty to decouple between physical and biological processes as observed by ocean color satellite data. This limitation hinders the quantification of bloom demise and its regulation by biological processes [5, 6], which has important consequences on the efficiency of the biological pump of carbon to the deep ocean [7–9].

Here, we address this challenge and quantify algal blooms' turnover using a combination of satellite and in situ data, which allows identification of a relatively stable oceanic patch that is subject to little mixing with its surroundings. Using a newly developed multisatellite Lagrangian diagnostic, we decouple the contributions of physical and biological processes, allowing quantification of a complete life cycle of a mesoscale (~10–100 km) bloom of coccolithophores in the North Atlantic, from exponential growth to its rapid demise. We estimate the amount of organic carbon produced during the bloom to be in the order of 24,000 tons, of which two-thirds were turned over within 1 week. Complementary in situ measurements of the same patch area revealed high levels of specific viruses infecting coccolithophore cells, therefore pointing at the importance of viral infection as a possible mortality agent. Application of the newly developed satellite-based approaches opens the way for large-scale quantification of the impact of diverse

environmental stresses on the fate of phytoplankton blooms and derived carbon in the ocean.

## Results and Discussion

Ocean color satellites have uniquely contributed to the study of phytoplankton blooms over a wide range of spatial and temporal scales, providing the means for a long-term synoptic view of the marine biosphere [1, 5, 10, 11]. Although commonly used to study early phases of the bloom, satellite quantification of the demise phase is still underexplored. A fundamental obstacle in applying satellite data to the study of bloom demise is the difficulty to decouple between biological processes (e.g., grazing, viral infection) occurring within the planktonic system and external physical forces (e.g., vertical and horizontal mixing) acting on the system.

Here, we unveil the underlying biological processes associated with phytoplankton bloom demise by defining a set of strict dynamical constraints that outline relatively steady environments that are subject to little mixing with their surroundings. Under these constraints, the bloom signature is only slightly affected by external physical forces, and its dynamics can be attributed to internal biological processes. We look to identify these conditions in a subset of mesoscale (~10–100 km) patches whose lifetime is comparable with that of the phytoplankton bloom. Separation between surface and deep water is achieved when both mixed layer depth and the patch surface area are kept relatively invariant. Typical patches that meet such conditions have a well-stratified water column, with a shallow and stable mixed layer, and are separated from their surroundings by transport barriers induced by the horizontal surface currents [12]. Meeting these conditions suggests that within the analyzed timescales, the volume is kept relatively unchanged as are the optical and dynamical properties.

We found these conditions to be met in a mesoscale phytoplankton patch that inhabited the North Atlantic during the summer of 2012 (Figure 1A). The patch was identified from satellite data as a distinct area of elevated concentrations of surface chlorophyll (Chl), embedded within a mesoscale anticyclonic eddy (Figure 1B). Patch boundaries were outlined based on the surface water bio-optical properties as regions of strong Chl gradient around the high Chl area (contour encircling the region of high Chl region in Figure 1B). Complementary information on the patch extension was extracted based on Lagrangian and Eulerian analysis of satellite-derived surface velocity fields. From a Lagrangian viewpoint, the patch was defined by the structure of Lagrangian coherent structures (LCSs) [13] from calculation of finite-size Lyapunov exponents (FSLEs) (Figure 1B). From an Eulerian viewpoint, the patch was outlined according to the core of the mesoscale eddy, as identified by the Okubo-Weiss (OW) parameter (similar to [12]).

The phytoplankton patch was fully exposed (i.e., not masked by clouds) in three satellite images (June 6, June 22, and July 2; days 158, 174, and 184, respectively) (Figure 2A; Figure S1 available online). The patch morphology, as outlined based on spatial gradients in the chlorophyll field, evolved from a ring (days 158 and 174) to a spiral (day 184), while

\*Correspondence: [ilan.koren@weizmann.ac.il](mailto:ilan.koren@weizmann.ac.il) (I.K.), [assaf.vardi@weizmann.ac.il](mailto:assaf.vardi@weizmann.ac.il) (A.V.)

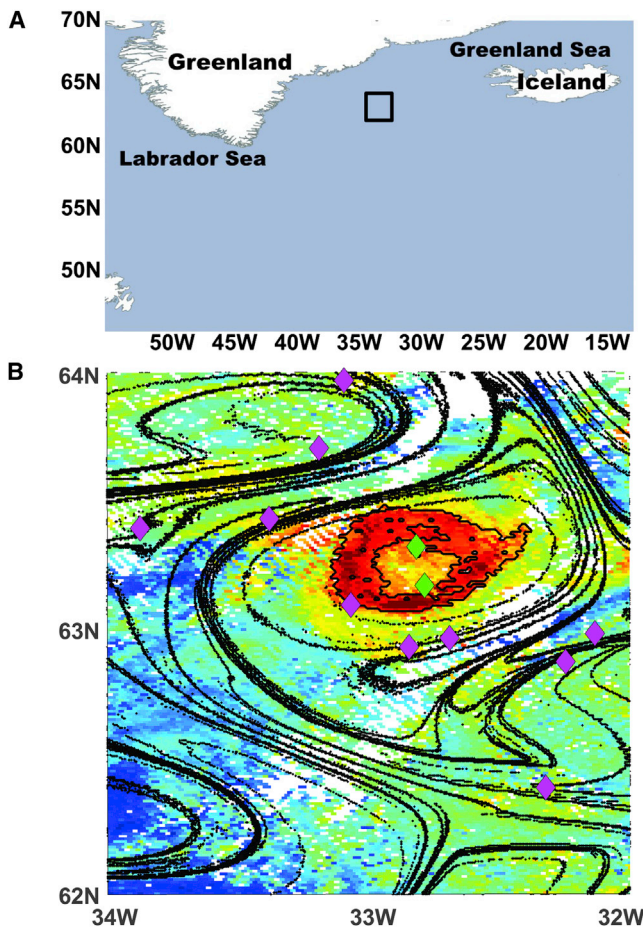


**Figure 1. Location and Biophysical Characteristics of the Study Area**  
(A) Location map. Black rectangle delineates the area shown in Figures 1B and 2.  
(B) Map of surface chlorophyll from June 22, 2012 (day 174), emphasizing the phytoplankton patch as a distinct area of high chlorophyll concentration. Thick black lines mark the main attracting Lagrangian coherent structures (LCSs) from calculation of finite-size Lyapunov exponents (FSLEs). To facilitate the presentation, we plotted only the highest 20% of FSLEs (for the entire FSLE field, see Figure 2C). Thin black contour outline region of strong Chl gradient is used to define patch boundaries. Magenta diamonds mark the position of Argo floats used for extracting the mixed layer depth in the patch vicinity. Green diamonds mark the location of the sampling stations.

conserving its surface area ( $1,336 \pm 63 \text{ km}^2$ ) and exhibiting little change in the location of its centroid (purple dot in Figures 2B and 2C). On days 174 and 184, the patch was characterized by a remarkable signature of particulate inorganic carbon (PIC), indicative of high coccolithophore abundance [14]. The fact that the bloom was dominated by coccolithophores is indicated by the high values of satellite-derived PIC and is validated by comparing early stages of coccolithophore blooms and the respective PIC satellite signature at other locations. Throughout its lifetime, the patch was encircled by attracting LCSs [13], separating it from surrounding waters (Figures 2A–2C) [15, 16]. Furthermore, during the study period, the patch was embedded within a well-stratified water column, with a relatively stable shallow mixed layer ( $16.6 \pm 5.3 \text{ m}$ , Figure 3A).

Time series of Chl, PIC, and particulate organic carbon (POC) were extracted by averaging satellite observations over the patch surface area (Figure 3). To reduce the uncertainty

associated with precise detection of the patch boundaries, for each time step, we sampled the patch over an area defined by two independent criteria: (1) a disc ( $r = 30 \text{ km}$ ) around the centroid of the patch, as identified based on the spatial distribution of surface chlorophyll, and (2) the core of the anticyclonic eddy, as delineated by the OW parameter [12]. The time series varied only slightly when the derivation was based on either of the two criteria (Figures 3B–3D, black and blue data points, respectively).

While maintaining a structure with conserved area and volume, the phytoplankton patch evolved through a 25-day life cycle that began with a fast growth phase, expressed by a 4-fold Chl concentration increase over a 17-day period (Figure 3B). Later, the patch went through a rapid demise phase, returning to Chl levels that were close to background approximately 8 days after reaching its peak. The POC levels closely followed the Chl trend, serving as a proxy for phytoplankton organic carbon [17] and further corroborating the pattern of coccolithophore bloom demise (Figure 3C).

The “boom and bust” pattern of bloom dynamics was also characterized by fluctuations in PIC levels, which is a marker for the  $\text{CaCO}_3$  plates (coccoliths) formed around the coccolithophore cells (Figure 3D). The  $\text{CaCO}_3$  optical signature in the water is a function of the concentration and viability of the coccolithophore cells. While the signature rises together with the cell concentration, detachment of plates from the cells increases their surface area and therefore their optical signature [14]. Because the coccoliths that are shed from dead cells have a slower sinking rate, their optical properties are likely to maintain a high surface PIC signature after cell lysis. This might explain the 2–3-day delay in onset of the decline phase and the lower decline rate in the PIC signal, with respect to that of Chl and POC (compare Figures 3B, 3C, and 3D). Most remarkably, during the 3 days following the bloom peak, Chl and POC levels declined rapidly to 48% and 62% of their peak values (as compared to total change throughout the bloom), whereas PIC levels hardly changed and maintained 95% of their peak value. Overall, the slower decline in PIC signature in comparison with that of Chl and POC ( $\sim 20$  days and  $\sim 10$  days from peak to background-like levels, respectively) is in agreement with previous field studies on *Emiliania huxleyi* natural blooms [18].

The stability of the mixed layer (Figure 3A), a typical characteristic of *E. huxleyi* blooms [19], indicates that the decrease in chlorophyll concentration does not result from dilution due to enhanced vertical mixing. Because the patch is isolated from its surroundings and is not subject to horizontal or vertical mixing, the abrupt demise is likely to reflect a rapid lysis of the phytoplankton cells comprising it.

To estimate the potential role of viral infection in the coordinated bloom demise, we conducted in situ measurements within the area delimiting the bloom approximately 5 days after the end of the demise phase (day 188, green dashed line in Figure 3). Measurements were taken within the patch in two separate profiles, hereafter referred to as cast 1 and cast 2 (Figure 4, black and blue lines, respectively). The two stations were characterized by a well-stratified water column with a shallow mixed layer of approximately 15 m (Figure 4A). Fluorescence profiles (Figure 4B) reveal a slightly thicker layer of chlorophyll, with maximum concentrations at around 17 m depth.

The average concentration of total dissolved inorganic nitrogen (DIN; Figure 4C) in the upper 15 m was  $4.3 \mu\text{M}$  in cast 1 and  $5.7 \mu\text{M}$  in cast 2. These values are in the range of concentrations observed in natural blooms [19], indicating that the

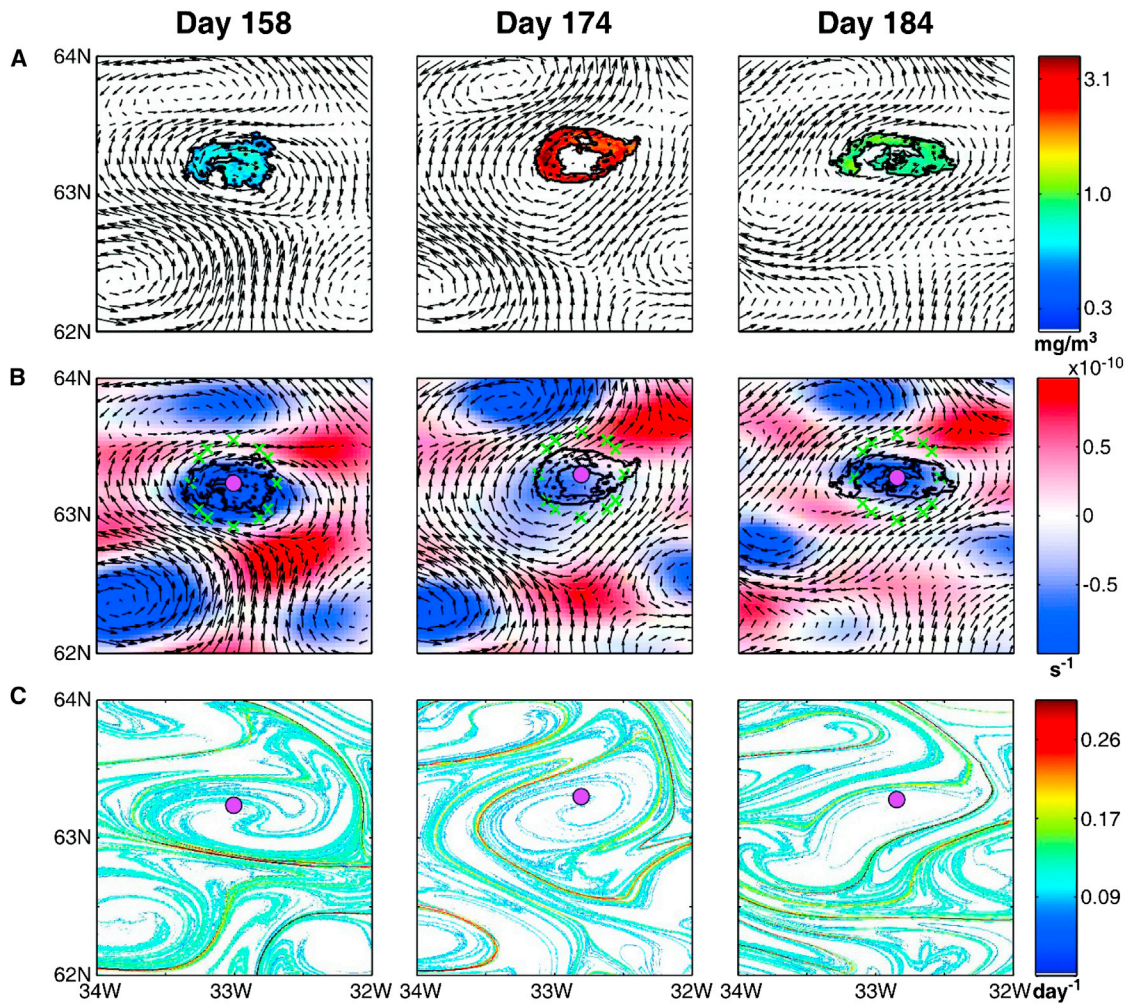


Figure 2. Phytoplankton Patch Morphology and Velocity Field Characteristics during Different Phases of the Bloom

(A) Chl cropped according to patch boundaries, which are identified as regions of strong gradients in the Chl field. Note the abrupt change in patch biomass as reflected in temporal variations in Chl values. For the equivalent images before cropping, see Figure S1.

(B) Okubo-Weiss (OW) parameter emphasizing the core of the eddy in which the patch is embedded as a region in the velocity field dominated by vorticity (negative OW) rather than deformation (positive OW).

(C) Attracting LCSs, which delineate transport barriers that separate between the patch and its surroundings. The images are from June 6, 2012, June 22, 2012, and July 2, 2012 (days 158, 174, and 184, respectively). Arrows represent the geostrophic surface currents. Purple dots mark the location of the patch centroid. Black contours delineate the patch boundaries. Green circles mark the 30 km disc around the patch centroid.

bloom demise is not likely to be driven by nitrogen limitation. The concentrations of phosphorus (as orthophosphate) were also measured, and an average of 0.5–1  $\mu\text{M}$  was measured throughout the water column of both casts (data not shown). These concentrations are higher than those previously reported for natural populations in a mesocosm setting [20], where the recorded maximal *E. huxleyi* cell numbers were higher than those measured in this study, suggesting that this oceanic bloom demise is not due to phosphorus limitation.

Maximal values of *E. huxleyi* cells ( $1 \times 10^3$  cells/ml in cast 1 and  $1.5 \times 10^3$  cells/ml in cast 2, Figure 4D), coccolith plates ( $8 \times 10^4$  coccoliths/ml, solid line in Figure 4E), and associated backscatter (dashed line in Figure 4E) were observed in the top 15 m. The elevated coccolith to cell ratio, which varied between 55 and 90, is indicative of a bloom in the demise stage [18, 21]. Based on flow cytometry analysis, we estimated that at this postbloom phase, *E. huxleyi* represented  $\sim 10\%$  of the total phytoplankton populations. Using flow cytometry

analysis, we also identified a distinct population of large viral-like particles (LVLPS), reaching  $2.5 \times 10^6$  LVLPS/ml (Figure S2). We compared the LVLPS with coccolithoviruses from cultures of *E. huxleyi* and found their flow cytometric signatures to be nearly identical. A similar range of abundance of *E. huxleyi* and its specific virus was found in the English Channel [22]. To further validate the presence of *Emiliania huxleyi* virus (EhV), which specifically infects only *E. huxleyi* cells, we quantified EhV DNA copies within coccolithophore cells by quantitative PCR (qPCR). Maximal concentrations of biomass-associated EhV in cast 1 and cast 2 were 860 viruses/cell and 230 viruses/cell, respectively (Figure 4F), which is well within the range of viral burst size seen in laboratory cultures and mesocosm experiments [23] and is therefore indicative of involvement of viral infection in the coordinated bloom demise.

We characterized that the bloom evolved through a 25-day life cycle, with an exponential growth phase and a rapid demise phase. Taking the area of the 30 km disc around the

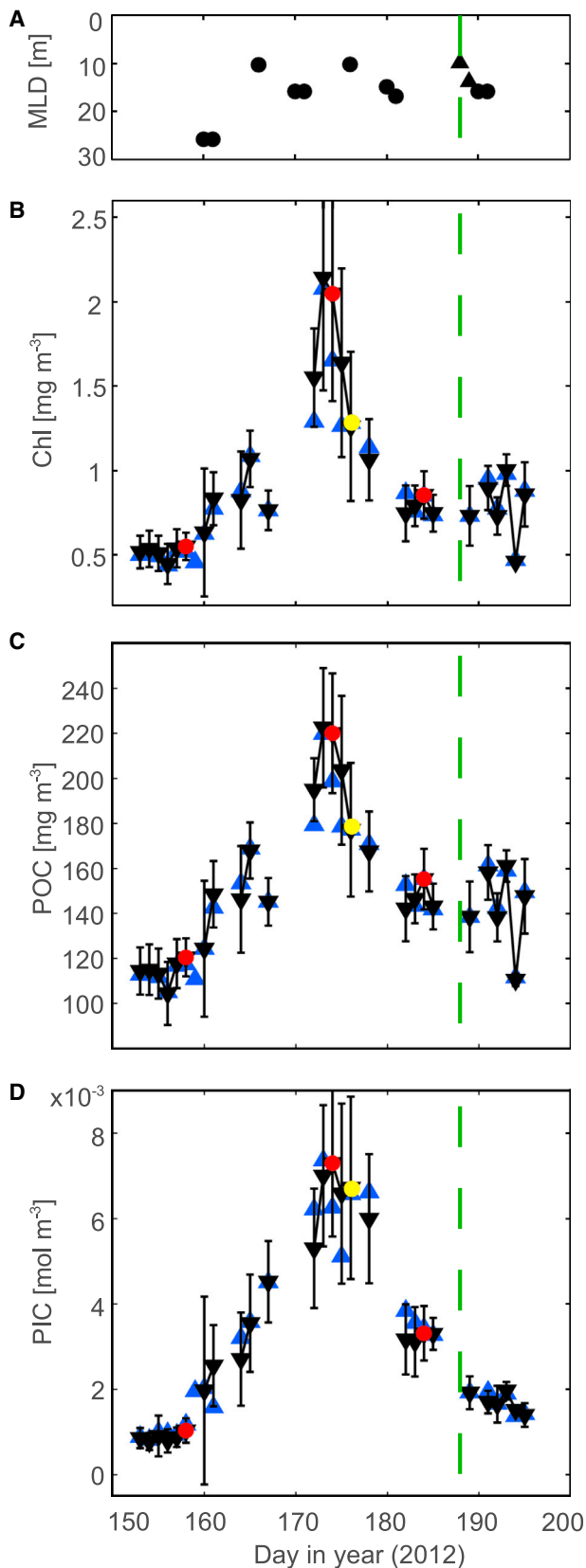


Figure 3. Temporal Changes in Physical and Biological Variables during Bloom Lifetime

(A) Changes in mixed layer depth (MLD) calculated from temperature profiles at a  $2^\circ \times 2^\circ$  ( $62^\circ\text{--}64^\circ$  N/ $32^\circ\text{--}34^\circ$  W) region overlapping the patch.

patch centroid (green circle in Figure 2B) as an approximation of the patch surface area, the euphotic depth of  $\sim 30$  m, and the average POC concentrations of  $\sim 140$   $\text{mg}/\text{m}^3$  (Figure 3C), we estimated the amount of organic carbon produced during the bloom to be in the order of 24,000 tons, of which two-thirds were turned over within one week of the demise phase. The demise phase was also characterized by profound deviation in residence time between the POC and PIC. This indicates a rapid cell lysis process that may be attributed to viral infection that was previously shown to induce programmed cell death-like degradation of cellular components [24, 25]. The low iron quota and phosphorus requirement of coccolithophores [19], combined with our in situ nutrient measurements, suggest that the bloom termination is not likely to be driven by nutrient limitation. Furthermore, recent mesocosm studies have shown that nutrient limitation did not lead to a sharp decline in *E. huxleyi* cell abundances as that caused by viral infection [20, 23].

Although we cannot rule out the importance of other major top-down regulating factors such as grazing, the high abundance of specific EhVs, combined with the rapid nature of the demise phase and deviation in residence time between organic and inorganic carbon, suggests that the bloom was regulated by marine viruses. Importantly, we measured high levels of intracellular concentrations of EhV within the coccolithophore cells (Figure 4F), which were well within the range of specific viral burst sizes measured in laboratory cultures and mesocosm experiments [23]. Interestingly, in cast 1, the highest intracellular EhV DNA concentrations were detected at a depth of 27 m, below the depth of maximal cell and coccolith abundances. This could indicate sinking of cells in the lytic stage of infection, possibly enhanced by transparent exopolymer particles produced during viral infection, which promotes cell aggregation and may stimulate carbon flux to the deep ocean [9].

Host-virus interaction during algal blooms can span more than ten orders of magnitude, from the individual cell ( $\sim 10^{-6}$  m) to mesoscale oceanic patches ( $\sim 10^5$  m); therefore, the lack of large-scale quantification of host-virus dynamics hinders our understanding of the ecological and biogeochemical role of viruses and virus-mediated processes in the oceans. Understanding the ecological and biogeochemical role of viruses and virus-mediated processes in the oceans is hindered by methodological constraints to evaluate in situ viral activity and by the lack of temporal and spatial quantifications of host-virus dynamics [8]. By enabling analysis of internal, biologically driven processes within mesoscale systems, satellite observations of these eddies will assist future studies to better evaluate the impact of diverse environmental stress conditions on the fate of phytoplankton blooms. Quantification of the relative contribution of each ecosystem

Temperature data are obtained from Argo floats (solid circles) and ship-board casts (triangles).

(B–D) Changes in concentrations of surface chlorophyll (Chl; B), particulate organic carbon (POC; C), and particulate inorganic carbon (PIC; D), derived from the MODIS instrument on board the Aqua satellite. Time series are extracted by averaging all available data over a disc ( $r = 30$  km) around the phytoplankton patch centroid (black data points) and over the area associated with the core of the eddy (blue data points). Error bars show SD of the data sampled over the disc. Red data points mark the benchmark time steps for which the patch is fully exposed (Figure 2). Yellow data points mark the end of the 3-day period during which Chl and POC decrease rapidly while PIC remains almost constant. Green dashed line marks the timing of the in situ sampling.

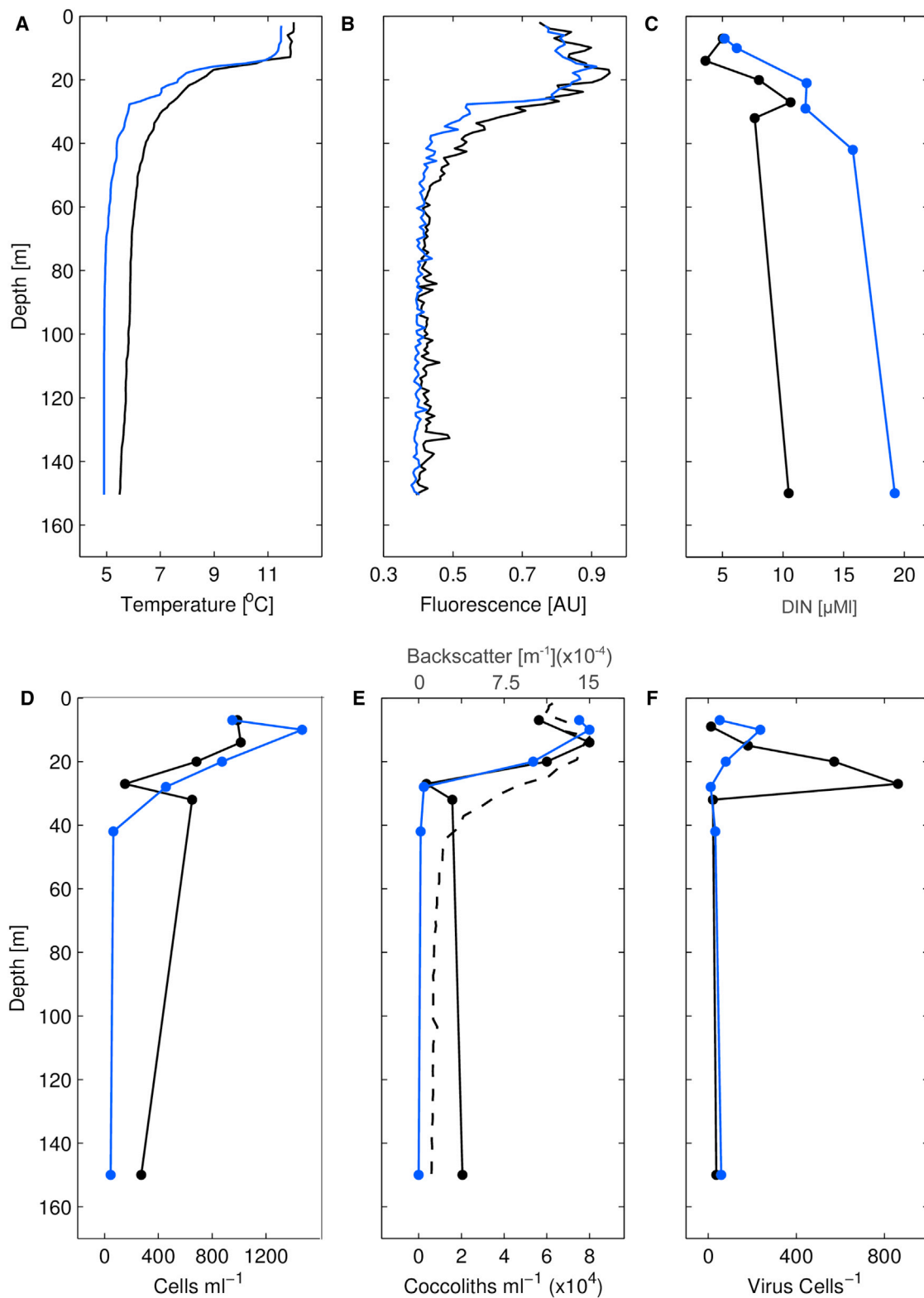


Figure 4. Vertical Profiles of Physical and Biological Variables

Profiles were measured in situ on July 6, 2012 at 09:12 local time at 63° 11' N/32° 47' W (cast 1, black lines) and at 19:07 local time at 63° 20' N/32° 49' W (cast 2, blue lines) during the coccolithophore bloom demise. Vertical variations in temperature (A), fluorescence (B), dissolved inorganic nitrogen (DIN) concentrations (C), *E. huxleyi* cell abundance (D), abundance of coccoliths (solid line) and backscatter (dashed line) (E), and concentration of coccolithoviruses in coccolithophore cells (F) measured by qPCR analysis are shown.

removal pathway (i.e., abiotic versus biotic) will improve our ability to incorporate these pathways into large-scale ecological and biogeochemical models. Precise and sensitive assessment of these large-scale processes will provide important insights into the effect of future global changes on the marine environment and the derived effects on the climate system.

#### Supplemental Information

Supplemental Information includes Supplemental Experimental Procedures and two figures and can be found with this article online at <http://dx.doi.org/10.1016/j.cub.2014.07.046>.

#### Author Contributions

A.V., D.S., I.K., and Y.L. wrote the manuscript. A.V., I.K., and Y.L. developed the Lagrangian framework used for diagnosing the bloom life cycle. S.E. and Y.L. processed and analyzed the satellite data. E.B. contributed to the interpretation of the satellite data. D.S. performed the qPCR analysis. U.S. performed the flow cytometry analysis. M.F. provided data on cells and coccolith abundance. K.D.B., C.L., and E.B. provided backscatter data. C.L. provided nutrient data. Y.R., M.T., S.S., G.R.D., M.J.L.C., A.M.M., B.A.S.V.M., and K.D.B. assisted in sampling the patch during the KN207-03 expedition.

#### Acknowledgments

We thank the captain and crew of the R/V Knorr for their tireless assistance and cooperation at sea, and we thank the Marine Facilities and Operations at the Woods Hole Oceanographic Institution for logistical support. We thank Avital Geva for fruitful discussion. A.V., D.S., U.S., and M.F. are supported by a European Research Council (ERC) Starting Grant (INFO TROPIC, grant #280991). A.V. is also supported by the Edith and Nathan Goldenberg Career Development Chair. I.K., Y.L., and M.T. are supported by the European Union's Seventh Framework Programme (FP7/2007-2013)/ERC (CAPRI, grant #306965). The research cruise was supported by NSF grant OCE-1061883 to K.D.B., B.A.S.V.M., A.V., M.T., and M.J.L.C.

Received: May 4, 2014

Revised: June 18, 2014

Accepted: July 16, 2014

Published: August 21, 2014

#### References

1. Field, C.B., Behrenfeld, M.J., Randerson, J.T., and Falkowski, P. (1998). Primary production of the biosphere: integrating terrestrial and oceanic components. *Science* 281, 237–240.
2. Behrenfeld, M.J., O'Malley, R.T., Siegel, D.A., McClain, C.R., Sarmiento, J.L., Feldman, G.C., Milligan, A.J., Falkowski, P.G., Letelier, R.M., and Boss, E.S. (2006). Climate-driven trends in contemporary ocean productivity. *Nature* 444, 752–755.
3. Boyce, D.G., Lewis, M.R., and Worm, B. (2010). Global phytoplankton decline over the past century. *Nature* 466, 591–596.
4. Valiela, I. (1995). *Marine Ecological Processes*, Second Edition (New York: Springer Media).
5. Behrenfeld, M.J., and Boss, E.S. (2014). Resurrecting the ecological underpinnings of ocean plankton blooms. *Annu. Rev. Mar. Sci.* 6, 167–194.
6. Bidle, K.D., and Falkowski, P.G. (2004). Cell death in planktonic, photosynthetic microorganisms. *Nat. Rev. Microbiol.* 2, 643–655.
7. Azam, F., and Malfatti, F. (2007). Microbial structuring of marine ecosystems. *Nat. Rev. Microbiol.* 5, 782–791.
8. Suttle, C.A. (2007). Marine viruses—major players in the global ecosystem. *Nat. Rev. Microbiol.* 5, 801–812.
9. Vardi, A., Haramaty, L., Van Mooy, B.A., Fredricks, H.F., Kimmance, S.A., Larsen, A., and Bidle, K.D. (2012). Host-virus dynamics and subcellular controls of cell fate in a natural coccolithophore population. *Proc. Natl. Acad. Sci. USA* 109, 19327–19332.
10. Behrenfeld, M.J., Westberry, T.K., Boss, E.S., O'Malley, R.T., Siegel, D.A., Wiggert, J.D., Franz, B.A., McClain, C.R., Feldman, G.C., Doney, S.C., et al. (2009). Satellite-detected fluorescence reveals global physiology of ocean phytoplankton. *Biogeosciences* 6, 779–794.
11. McClain, C.R. (2009). A decade of satellite ocean color observations. *Annu. Rev. Mar. Sci.* 1, 19–42.
12. Lehahn, Y., d'Ovidio, F., Lévy, M., Amitai, Y., and Heifetz, E. (2011). Long range transport of a quasi isolated chlorophyll patch by an Agulhas ring. *Geophys. Res. Lett.* 38, L16610.
13. Haller, G., and Yuan, G. (2000). Lagrangian coherent structures and mixing in two-dimensional turbulence. *Physica D* 147, 352–370.
14. Balch, W.M., Gordon, H.R., Bowler, B.C., Drapeau, D.T., and Booth, E.S. (2005). Calcium carbonate measurements in the surface global ocean based on Moderate-Resolution Imaging Spectroradiometer data. *J. Geophys. Res.* 110, C07001.
15. Lehahn, Y., d'Ovidio, F., Le'vy, M., and Heifetz, E. (2007). Stirring of the northeast Atlantic spring bloom: a Lagrangian analysis based on multi-satellite data. *J. Geophys. Res.* 112, C08005.
16. d'Ovidio, F., De Monte, S., Alvain, S., Dandonneau, Y., and Lévy, M. (2010). Fluid dynamical niches of phytoplankton types. *Proc. Natl. Acad. Sci. USA* 107, 18366–18370.
17. Behrenfeld, M.J., Boss, E., Siegel, D.A., and Shea, D.M. (2005). Carbon-based ocean productivity and phytoplankton physiology from space. *Global Biogeochem. Cycles* 19, GB1006.
18. Holligan, P.M., Viollier, M., Harbour, D.S., Camus, P., and Champagne-Philippe, M. (1983). Satellite and ship studies of coccolithophore production along a continental shelf edge. *Nature* 304, 339–342.
19. Tyrrell, T., and Merico, A. (2004). *Emiliania huxleyi*: bloom observations and the conditions that induce them. In *Coccolithophores: From Molecular Processes to Global Impact*, H.R. Thierstein and J.R. Young, eds. (Berlin Heidelberg: Springer-Verlag), pp. 75–97.
20. Kimmance, S.A., Allen, M.J., Pagarete, A., Martínez Martínez, J., and Wilson, W.H. (2014). Reduction in photosystem II efficiency during a virus-controlled *Emiliania huxleyi* bloom. *Mar. Ecol. Prog. Ser.* 495, 65–76.
21. Balch, W.M., Kilpatrick, K.A., and Holligan, P.M. (1993). Coccolith formation and detachment by *Emiliania huxleyi* (Prymnesiophyceae). *J. Phycol.* 29, 566–575.
22. Wilson, W.H., Tarran, G.A., Schroeder, D., Cox, M., Oke, J., and Malin, G. (2002). Isolation of viruses responsible for the demise of an *Emiliania huxleyi* bloom in the English Channel. *J. Mar. Biol. Assoc. U. K.* 82, 369–377.
23. Bratbak, G., Egge, J.K., and Heldal, M. (1993). Viral mortality of the marine alga *Emiliania huxleyi* (Haptophyceae) and termination of algal blooms. *Mar. Ecol. Prog. Ser.* 93, 39–48.
24. Vardi, A., Van Mooy, B.A., Fredricks, H.F., Pendorf, K.J., Ossolinski, J.E., Haramaty, L., and Bidle, K.D. (2009). Viral glycosphingolipids induce lytic infection and cell death in marine phytoplankton. *Science* 326, 861–865.
25. Bidle, K.D., Haramaty, L., Barcelos e Ramos, J., and Falkowski, P. (2007). Viral activation and recruitment of metacaspases in the unicellular coccolithophore, *Emiliania huxleyi*. *Proc. Natl. Acad. Sci. USA* 104, 6049–6054.